5M.2 Fog and Low Clouds in the Coastal Zone

William T. Thompson, Stephen D. Burk, and Shouping Wang

Naval Research Laboratory
Monterey, California

1. INTRODUCTION

The formation of fog over the ocean has been investigated by numerous authors*. The importance of transient weather systems in maritime fog formation is discussed by Leipper (1994) and Lewis et al. (2003) while the role of radiative cooling at low levels is emphasized by Roach (1995) and Leipper (1994). Another mechanism leading to fog at the surface is the lowering of stratus cloud layers. Formation of fog in coastally trapped disturbance (CTD) events has received relatively little attention in the literature. This is in contrast to fog in the vicinity of the east coast of the U. S. which is fairly well documented. In our examination of the clouds in the coastal zone, we find an interesting relationship between the surface latent and sensible heat fluxes and the horizontal extent of the fog. And, using an approach suggested by Lewellen et al. (1996), we generalize this examination to study the integrated contribution of liquid water (i.e., latent heat) to total buoyancy production

In the present study, we compare and contrast two fog events; the first occurring in conjunction with a CTD along the west coast of the U. S. on 15 June 2000 and the second occurring over the area south and east of Cape Cod, MA on 21 August 2003 during the Coupled Boundary Layers Air-Sea Transfer (CBLAST) experiment. In both cases, we use the COAMPS®* mesoscale model to simulate the events.

2. MODEL DESCRIPTION

The COAMPS® model is a nonhydrostatic mesoscale model, using multiple nests having different horizontal resolution. It features a full suite of physical parameterizations, including schemes for radiation, cloud microphysics, and turbulence. Time-dependent lateral boundary conditions are obtained from the Navy global model (NOGAPS) and applied to the boundaries of the outermost nest. Lateral boundary conditions on inner nests are supplied by outer nests. Data assimilation is accomplished using a scheme which, in the absence of observational data, retains horizontal and vertical structure developed in the previous forecast in the initial conditions of a subsequent forecast. Where observational data are available, these data are incorporated into the initial conditions using an increment formed between the observational analysis and the previous forecast. The model is described in more detail by Hodur et al. (2002).

In the present study, the model is run in a triply-nested mode with 45 levels in the vertical extending from the surface to ~ 30 km with the first grid point at 10 m. There are 5 levels below 200 m and spacing stretches to several km at higher elevations. Given this distribution of points, there are 20 levels in the lowest 1 km.

In the west coast case, the nests have horizontal resolutions of 45 km, 15 km, and 5 km. The innermost nest consists of 181X181 grid points extending from 31^{o} N to 39^{o} N and form 117^{o} W to 126^{o} W (Fig. 1). Data assimilation is performed for three days prior to the period of interest (0500 – 1700 LT 15 June. This case has been examined in detail by Thompson et al. (2005).

In the east coast case, horizontal resolutions are 27 km, 9 km, and 3 km. The innermost nest consists of 91X91 points extending from 39.9^{o}N to 42.4^{o}N and from

* Corresponding Author: William T. Thompson, Naval Research Laboratory, Monterey, CA 93943, thompson@nrlmry.navy.mil

* COAMPS is a registered trademark of the Naval Research Laboratory

72.3°W to 69.2°W (Fig. 2). Data assimilation is performed for two days prior to the period of primary interest using a sequence of four 12 h forecast beginning 2000 LT 19 August 2003.

3. SYNOPTIC OVERVIEW

3.1 CTD Case

The propagation of the CTD occurred over a 60 h period, from 0500 LT 13 June to 1700 LT 15 June 2000. The sea fog first appeared in the California Bight and progressively moved northward to Pt. Arena. On 12-13 June, a strong pressure ridge built and moved into the Pacific Northwest. Northeast winds in the 850/700 layer were in evidence over the north and central California coast. The subsidence and associated adiabatic warming led to record breaking temperatures in the central valley extending into southern California. The satellite imagery on 14 June (not shown) indicated a wide swath of clear sky off the California coast - a response to the strong subsidence and offshore flow of warm, dry air. The warm, stable boundary layer to the north with the cool, cloudy boundary layer near Pt. Conception results in a reversal in the alongshore pressure gradient. The CTD then propagates to the north along the coast with a reversal in wind direction followed by a narrow tongue of fog and low clouds along the coast.

The sea surface temperature (SST) distribution shows low temperature along the coast with still lower temperature to the north (north of San Francisco).

3.2 CBLAST Case

In this case, the synoptic situation is relatively quiescent as a slowly moving surface anti-cyclone moves offshore over the mid-Atlantic coast on 19-20 August 2003 and remains centered ~250 km offshore during the day on 21 August. This results in relatively weak SW flow over the CBLAST area during the day. Fog forms near the SW corner of the domain and transits the area from SW to NE.

The SST distribution in this case shows a tongue of relatively warm temperatures in the western ~1/3 of the domain with a cold pool near the eastern boundary. Along a line passing through the warm tongue and cold pool, temperature deceases 10 °C over ~150 km.

4. RESULTS

4.1 Fog and Low Cloud Characterization

Shown in Fig. 3a is the region over which the COAMPS® cloud liquid water mixing ratio at 10 m elevation exceeds 0.01g/Kg (which we term the" fog footprint") in the CTD case at 1700 LT 15 June. Experience with the model shows that using this rather low threshold value guarantees that all of the fog, no matter how tenuous, will be included in the fog footprint. The fog extends from just south of Pt. Arena to the northern portion of the Southern California Bight and offshore to near 33°N, 125°W. To the south of the shaded region, fog lifts away from the surface to form low clouds which extend nearly to the southern boundary of the domain east of 122°W and to the western boundary of the domain near 32°N. The extent of low clouds is shown in Fig. 3b, which depicts the 0.01 g/Kg isosurface of cloud liquid water. In this depiction, all areas in which cloud liquid water is nonzero are shown with no regard to elevation. Thus, this figure shows the areal extent of both fog and low clouds. Shading in this figure indicates variations in the elevation of the top of the layer in which cloud liquid water mixing ratio is greater than or equal to 0.01 g/Kg (the elevation deviations are relatively subtle except at the leading edge of the fog). Comparison of Fig. 3a to Fig. 3b shows extensive low cloudiness to the south and throughout the Southern California Bight.

Early in the CTD propagation phase, more rapid advancement of the fog tongue in the model is consistent with the faster than observed propagation of the wind shift along the central portion of the coast (not shown). As the wind shift slows north of Monterey, the model fog tongue propagation slows and the observed fog tongue approaches and then moves beyond the modeled position.

A depiction similar to that in Fig. 3 but for the CBLAST case is shown in Fig. 4a, b). At this time, a relatively wide band of fog extends across most of the domain south of

the land area and to within 30-40 km of the southern boundary of the domain. Comparison on Fig.s 4a and 4b shows that the low clouds are more extensive, extending to the southern boundary. As in the CTD case, the fog rises above the surface to the south.

4.2 *Fog and Cloud Layer Moist Thermodynamic Processes*

In order to characterize the contribution of the integrated effect of latent heat release to the integral of total buoyancy flux generation (following Lewellen et al. 1996), we define the ratio of the liquid water flux to the total buoyancy flux:

$$\beta = \frac{(\frac{L_v\theta}{c_pT} - 1.61\theta_o)\int \langle w'q'_l \rangle dz}{\int \langle w'\theta_v' \rangle dz} \quad (1)$$

where $<w'\theta_v>$ is the total buoyancy flux and $<w'q_l'>$ is the turbulent liquid water flux. In the physics option of COAMPS® used here, the buoyancy flux and liquid water flux may be written as:

$$< w'\theta_v^{'}'>= \beta_w < w'q_w' > + \beta_l < w'q_l^{'}> + \beta_T < w'\theta_l'^{'} > \quad (2)$$

$$< w'q_l'>= R'(a < w'q_w'> - b < w'\theta_l'>) \quad (3)$$

and where $<w'q_w'>$ is the flux of total moisture and $<w'\theta_l'>$ is the flux of liquid water potential temperature, R' is a function of the statistical cloud fraction R (obtained from a cloud fraction scheme using a Gaussian pdf), Q_s is the saturation mixing ratio, L_v is the latent heat of vaporization, c_p is specific heat at constant pressure, and the values of a, b, β_T, β_l, and β_w are given in Yamada (1978) and Yamada and Mellor (1979).

Following Stage and Businger (1981), we define the denominator of the integral in equation (1) so as to include only net positive buoyancy flux (Lewellen et al. used the total buoyancy flux, however, using the total buoyancy flux produced considerable high-frequency variability in our results because the denominator can get quite small in some regions).

4.2.1.CTD CASE

In the CTD case the results showed that, over most of the region of the fog footprint (northern~2/3), the ratio of liquid water flux to total buoyancy generation is negative (Fig.1). The interpretation of the negative values of β in the fog layer is that the liquid water flux is negative due to the dominance of cloud top radiative cooling over entrainment and evaporation. Negative values of liquid water flux can also be inferred in the investigation of Lewellen and Lewellen (1998; their Figure 13 and personal communication) in cases in which the humidity jump at the inversion was small.

Shown in Fig. 5 are 12 h forecast vertical profiles from a point near the center of the fog footprint (35.2°N, 122°W; see point 1 in Fig.1). This point is located within the portion of the fog footprint in which $\beta<0$. The families of profiles show the vertical distribution of the thermo-dynamic fluxes (to this point, the discussion has been centered on integral quantities). The profiles are identified by letter; A is the total water flux term (term 3 on the RHS of equation 2), B is the liquid water flux term (term 2 on the RHS of equation 2), C is the liquid water potential temperature flux term (term 1 on the RHS of equation 2), and D is the virtual buoyancy flux (the LHS of equation 2); thus, A, B, and C sum to D.

At this location, the depth of the boundary layer is ~200 m. The total water flux term (A) is negligible and the liquid water flux distribution (B) is such that the integral is negative as expected since $\beta<0$ at this location. The liquid water flux is, however, positive in the upper portion of the cloud. This is the result of entrainment of warm, dry air (as indicated by the liquid water potential temperature flux (C)) and evaporation of cloud water. The sign of the liquid water flux is opposite to that of the liquid water potential temperature flux (lwptf). The lwptf is negative due to entrainment of warm air. The liquid water flux is positive due to evaporation and thus counteracts, to some extent, the destruction of buoyancy by entrainment. Radiative flux divergence at cloud top results in positive lwptf and negative liquid water flux. Note, however, that the effect of radiative cooling on the fluxes is seen in the lower portion of

the cloud in spite of the fact that the cooling takes place in the upper few 10's of meters of the cloud. Destabilization of the mixed layer by radiative cooling results in vigorous turbulent mixing.

To examine the distribution of the fluxes as the LCL lifts off the surface, profiles are examined at several times at a location near the edge of the fog footprint (33.3^{o}N, 122^{o}W; see point 2 in Fig. 1). At this location, the fog lifts off the surface at hour 9. Profiles at hour 9 are shown in Fig, 6. The boundary layer depth is 260 m at hours 3 and 6 and ~350 m at hours 9 and 12. Note that the distribution of the liquid water flux is such that the integral of this quantity is negative at hours 3 and 6 and positive at hours 9 and 12 (i.e., the sign of β changes with time).

From the vertical distribution of the fluxes, it is evident that significant entrainment occurs at hour 9 as the fog lifts away from the surface. The magnitude of the negative virtual buoyancy flux in the cloud layer at this time is significantly larger (by nearly a factor of three) than at the other times shown, although the effect of liquid water flux in counteracting virtual buoyancy destruction is also largest at this time. Thus, the correlation between liquid water potential temperature flux and liquid water flux, i.e., entrainment warming/drying and evaporation of cloud water, are the primary processes determining when the cloud base will lift off the surface to form low clouds.

4.2.2 CBLAST CASE

In the CBLAST case, in contrast to the CTD case, the distribution of β shows a banded structure, with alternating bands of positive and negative (or near zero) values (Fig. 2). These bands are coincident with changes in the topography of the cloud top, demonstrating a strong connection between β and entrainment. Positive bands in β correspond to deepening of the cloud layer while negative or near 0 bands wherein negative liquid water flux reduces total buoyancy flux correspond to areas in which the depth of the cloud is not changing. The temporal evolution of the β field is also quite dramatic: initially, the field is flat and near 0 and, as the clouds advance from SW to NE, larger values of β move with the low cloud edge and the banded structure begins to appear.

Shown in Fig.s 7 and 8 are profiles from two locations in the CBLAST domain. The first point (point 1 in Fig. 2) is located in an area of extremely low SST while the second (point 2 in Fig. 2) is near the SW corner of the domain. Comparison on Fig. 9 with Fig. 7 (also in a region of relatively low SST) for the CTD case shows that, in the layer above the large peak values in liquid water flux and lwptf, there are small positive values of liquid water flux and negative values of lwptf and total buoyancy in the CTD case which are absent from the CBLAST case. These small fluxes are associated with entrainment of warm, dry air. Thus, there is very little evidence of entrainment at this location in the CBLAST case. Examination of the model vertical profile of potential temperature at several different times (not shown) indicates that a shallow mixed layer overlying a stable surface layer results from strong radiative cooling at the top of the fog (~3 ^{o}C at ~200 m elevation) rather than from entrainment. Note also the negative "tail" of the distribution in Fig. 9 associated with the stable surface layer at this location. Shown in Fig. 10 are profiles from a location at which significant entrainment has taken place and the fog lifts away from the surface shortly after the time shown. Thus, the situation is quite similar to that shown in Fig. 8. The distribution of fluxes in Fig. 10 is quite similar to those shown in Fig. 8, although the magnitudes are substantially larger. Just as in Fig. 8, the liquid water flux is near zero in the subcloud layer and becomes strongly positive in the cloud layer due to evaporation of cloud water resulting from entrainment of dry air. The lwptf is positive in the subcloud layer and becomes strongly negative in the cloud layer due to entrainment of warm air.

5. CONCLUSIONS

Conclusions at this stage are somewhat preliminary as analysis of the CBLAST results is ongoing. Nonetheless, some intriguing differences between the west coast CTD case and the east coast CBLAST case are apparent. These include the spatial distribution of the contribution of latent heat to buoyancy generation, the strong connection between this ratio and entrainment, and differences in the evolution

of structure in the stable boundary layer over cold SST's.

Several sensitivity studies have been conduction in connection with the CTD case. Similar sensitivity structures for the CBLAST case should provide further insight.

Acknowledgements: This research was supported by the Office of Naval Research Program Element 0601153N and under Program Element 0602435N

REFERENCES

Hodur, R. M., J. Pullen, J. Cummings, X. Hong, J. D. Doyle, P. Martin, and M. A. Rennick, The coupled ocean/atmosphere mesoscale prediction system (COAMPS), *Oceanography, 15***,** 88-89, 2002.

Leipper, D., Fog on the U. S. West Coast: A review*, Bull. of the American Met. Soc*., *75*, 229-240, 1994.

Lewellen, D. C. and W. S. Lewellen, Large-eddy boundary later entrainment, *J. Atmos. Sci*., *55*, 2645-2665, 1998.

-----, -----, and S. Yoh, Influence of Bowen Ratio on boundary layer cloud structure, 1996.

Lewis, J., Koracin, D., Rabin, R., and Businger, J. , Sea fog along the California coast: Viewed in the context of transient weather systems, *J. Geophys. Res.* (Atmospheres), *108*, 4457-4474, 2003.

Roach, W., Back to basics: Fog: Part 3 – The formation and dissipation of sea fog. *Weather, 30*, 80-84, 1995.

Stage. S. A. and J. A. Businger, A model for entrainment into a cloud-topped marine boundary layer. Part 1: Model description and application to a cold-air outbreak episode, *J. Atmos. Sci*., *38*, 2213-2229, 1981.

Yamada, T. , A three-dimensional second-order closure numerical model of mesoscale circulations in the lower atmosphere: Description of the basic model and application to the simulation of the environmental effects of a large cooling pond. Argonne National Laboratory Report ANL/RER-78-1, Argonne, IL. 67 pp., 1978.

----- and G. L. Mellor, A numerical simulation of BOMEX data using a turbulence closure model coupled with ensemble cloud relations, *Quart. J. Roy. Meteor. Soc*., *105***,** 915-944, 1979.

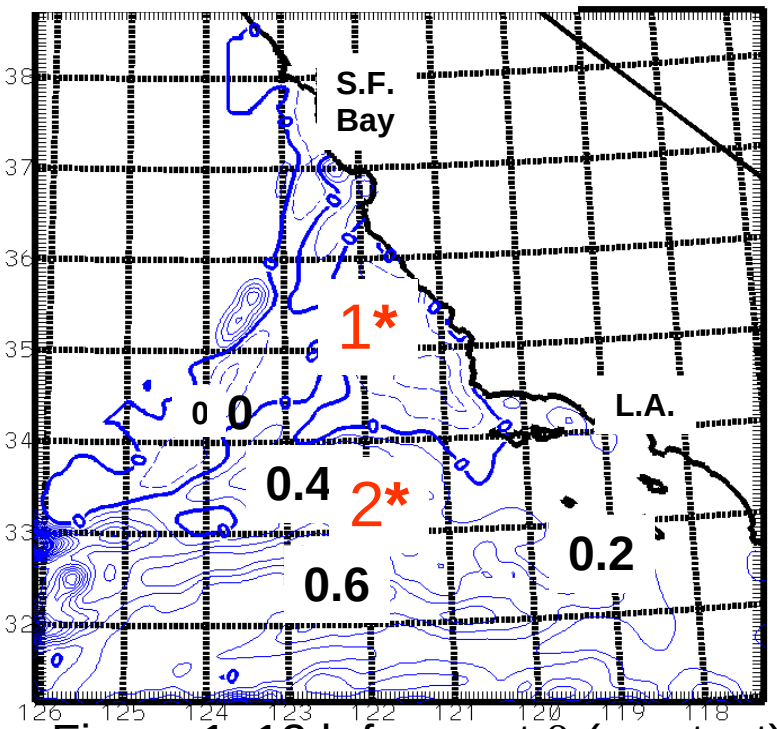

Figure 1. 12 h forecast β (see text) valid 1700 LT 15 June 2000. The location of points 1 and 2 is shown.

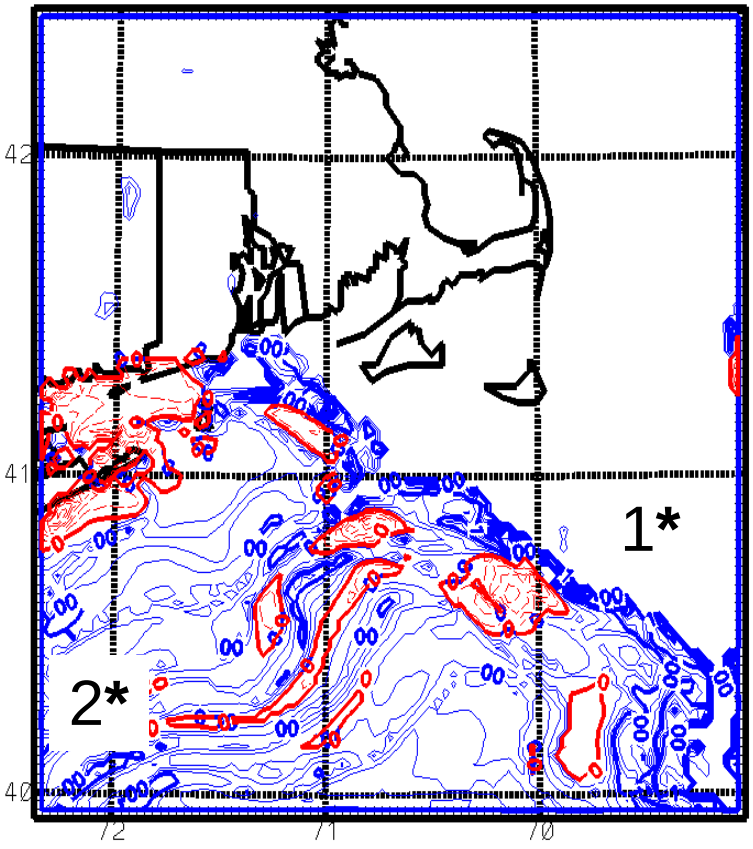

Figure 2. 16 h forecast β (see text) valid 1600 UTC 21 August 2003.

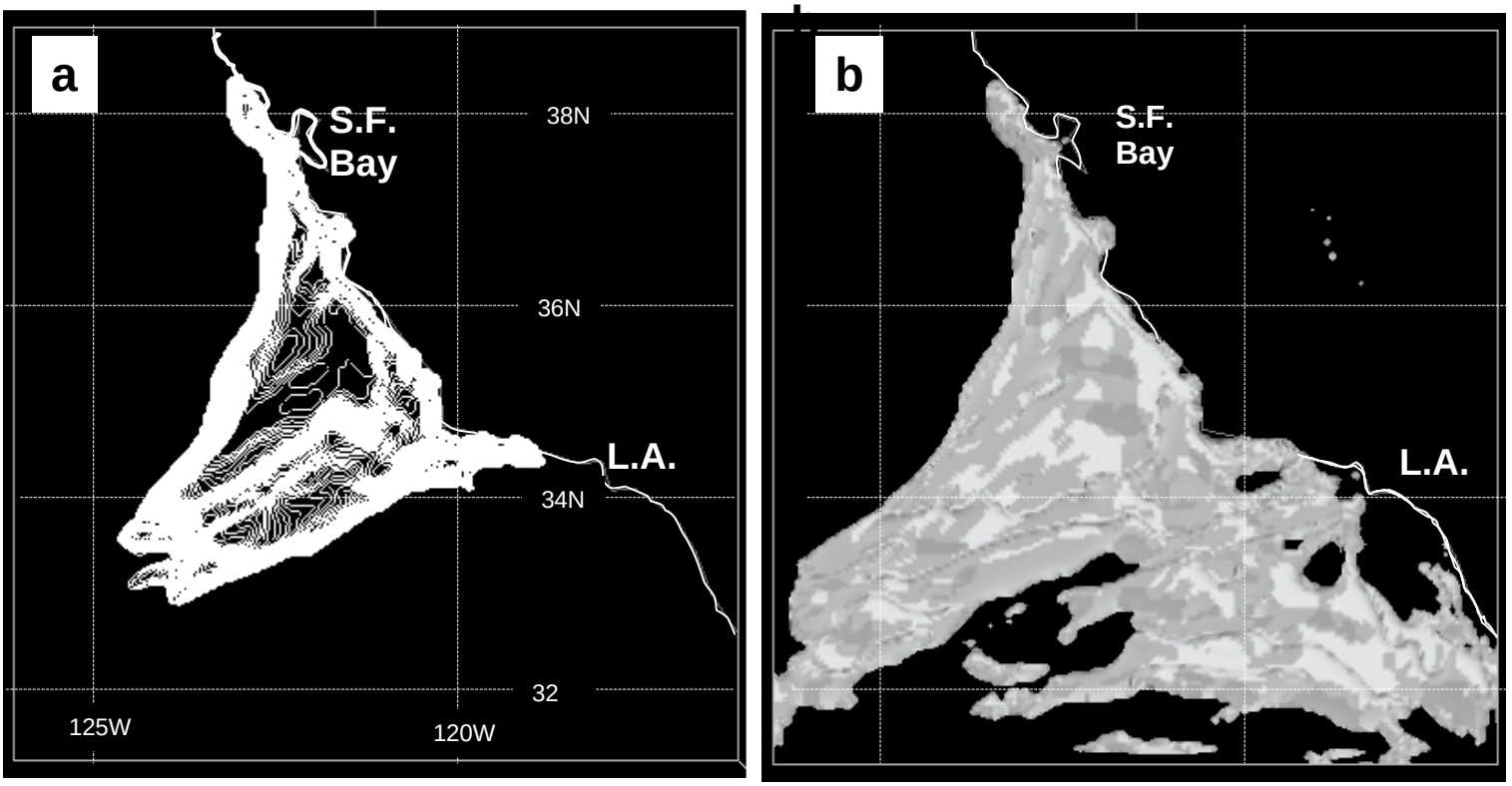

Figure 3 a)12 h forecast cloud liquid water at 10 m elevation (fog footprint) and b) isosurface of cloud liquid water (=0.01 g Kg^{-1}) valid 1700 LT 15 June 2000.

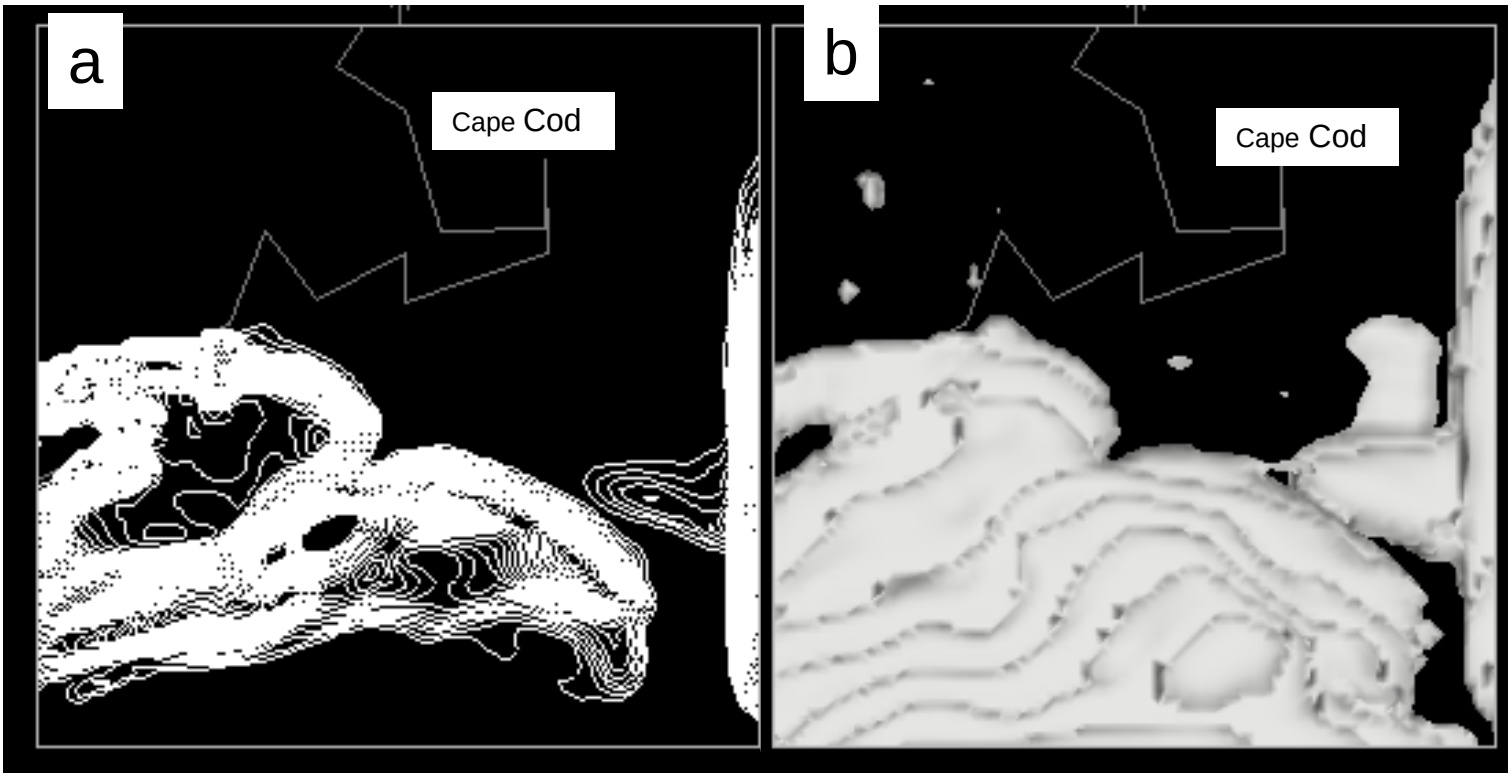

Figure 4. As in Fig. 3 but valid 1200 LT 21 August 2003

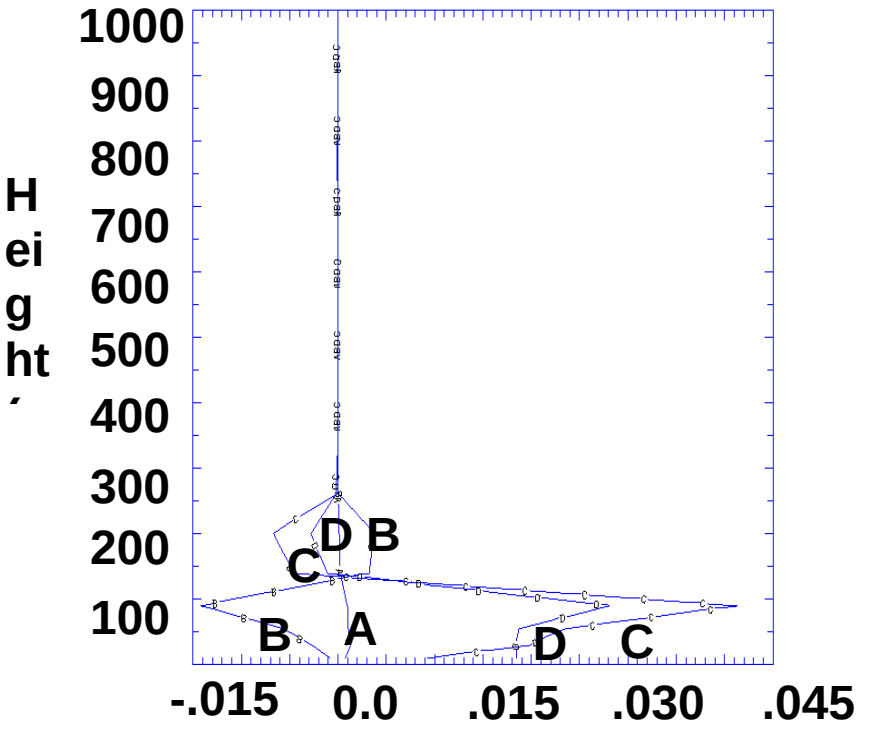

Figure 5. 12 h forecast profiles of buoyancy Components for point 1 (CTD**)**

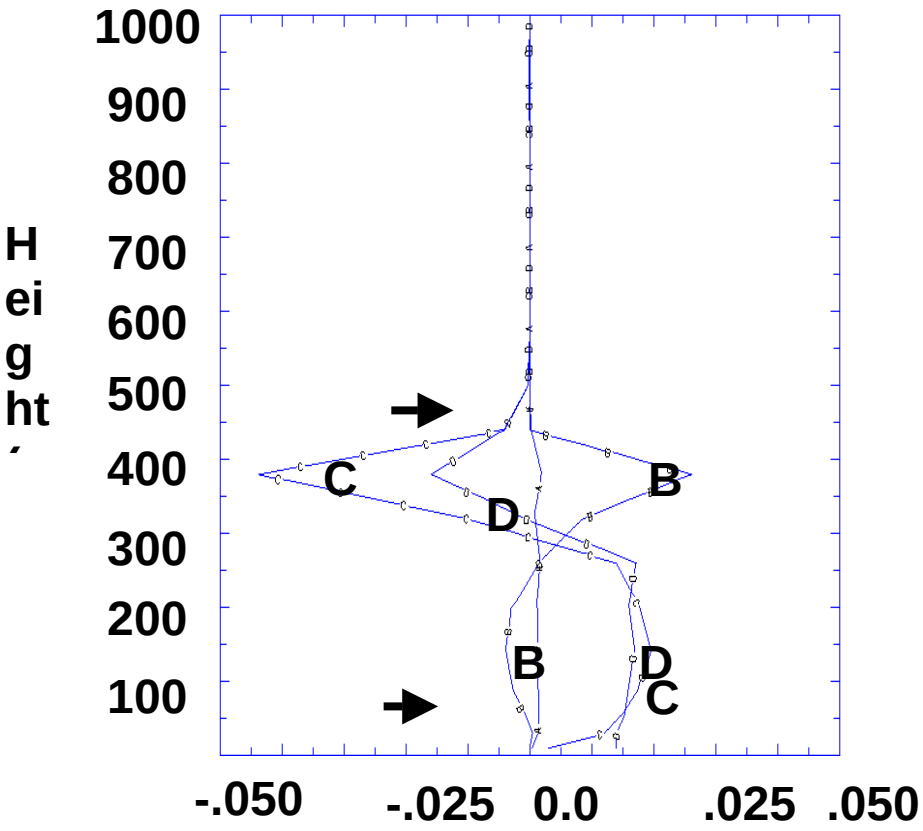

Figure 6 As in Fig 5 but for

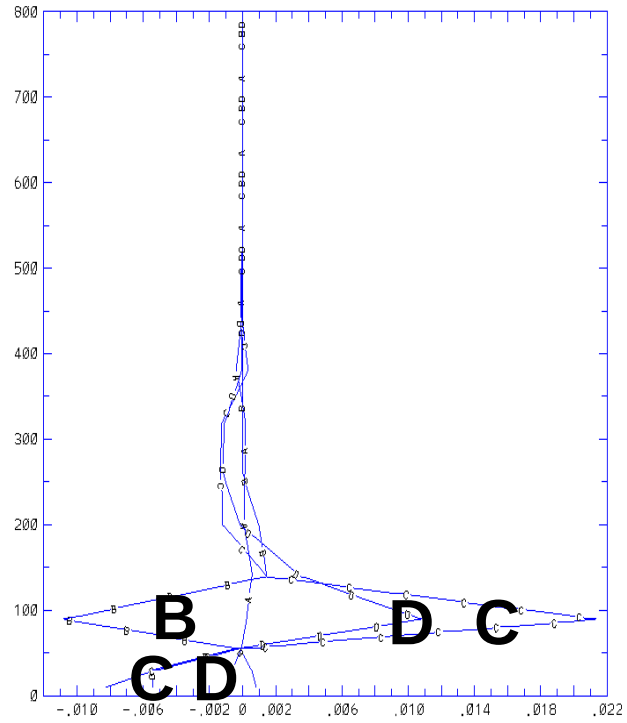

Figure 7. 16 h forecast profiles of buoyancy flux components for point 1 (CBLAST)

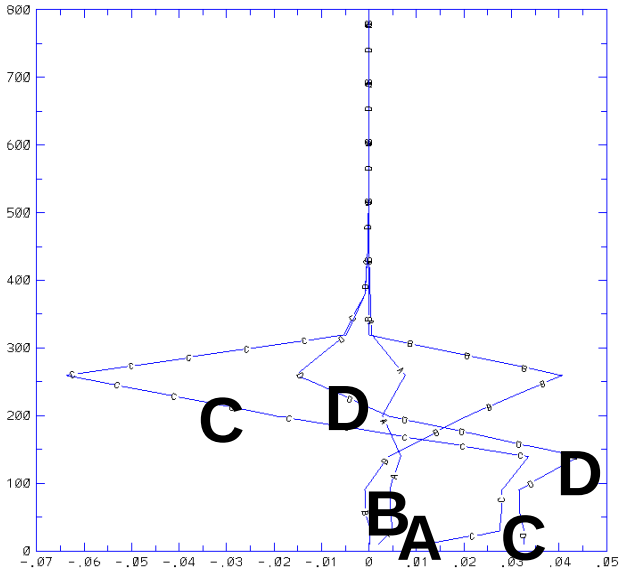

Figure 8. As in Fig. 7 but for point 2.